

Waves in Random and Complex Media

ISSN: (Print) (Online) Journal homepage: <https://www.tandfonline.com/loi/twrm20>

Von Kármán viscous pump of rotating disk in a magnetized Maxwell fluid with Joule heating

Kotha Gangadhar, R. Edukondala Nayak, Pallamkuppam Vinodh Kumar & Ali J. Chamkha

To cite this article: Kotha Gangadhar, R. Edukondala Nayak, Pallamkuppam Vinodh Kumar & Ali J. Chamkha (2023): Von Kármán viscous pump of rotating disk in a magnetized Maxwell fluid with Joule heating, Waves in Random and Complex Media, DOI: [10.1080/17455030.2023.2226240](https://doi.org/10.1080/17455030.2023.2226240)

To link to this article: <https://doi.org/10.1080/17455030.2023.2226240>



Published online: 20 Jun 2023.



Submit your article to this journal [↗](#)



Article views: 15




View related articles [↗](#)



View Crossmark data [↗](#)



Von Kármán viscous pump of rotating disk in a magnetized Maxwell fluid with Joule heating

Kotha Gangadhar ^a, R. Edukondala Nayak^a, Pallamkuppam Vinodh Kumar^b and Ali J. Chamkha^c

^aDepartment of Mathematics, Acharya Nagarjuna University Campus, Ongole, India; ^bSchool of Electrical Engineering, Vellore Institute of Technology, Vellore, India; ^cFaculty of Engineering, Kuwait College of Science and Engineering, Safat, Kuwait

ABSTRACT

The current investigation is concentrated on the constant MHD flow of an electrically charged Maxwell fluid across a radially elastic spinning disc in the presence of a uniform magnetic field. The problem is a generalization of the prevalent von Kármán viscous pump for configurations with or without a stretchy disc. The plane fluid content is controlled using an isothermal approach of homogeneous-heterogeneous processes. Non-linear thermally radiative heat transfer's effects on heat transference properties are investigated. Viscous dissipation and Joule heating are two other factors to consider in the energy equation. The von Kármán adaptations are used to build non-dimensional Navier-Stokes models, which are then, calculated using the *bvp4c* method. The torque, wall shear stresses, vertical pressure velocity, and heat transfer proportion are all determined. In addition, a statistical method is used to determine the connection between factors and the flow system's physical characteristics. Increasing the radiation parameter lowers the heat transmission rate at the disk's layer is a key finding. When homogeneous and heterogeneous reactants are reinforced at the same time, a significant observation is made that minimizes species concentration behaviors. Fluid flow caused by spinning discs is used in thermal transfer systems for nuclear propulsion devices.

ARTICLE HISTORY

Received 6 December 2021

Accepted 8 May 2023

KEYWORDS

Rotating disk; Joule heating; non-linear radiative heat flux; heat source; homogeneous-heterogeneous chemical change

1. Introduction

Researchers have been inspired by the growing importance of non-Newtonian fluid mechanics rheology in polymers, oil, chemicals, and food processing. Non-Newtonian fluid models may be used to simulate the fluid flow behavior often found in industries, such as bio, polymeric, and hydraulic fluids, as well as different mixes. In viscoelastic fluids, shear stress is the functional storage displacement. After the applied shear force is removed from these fluids, the percentage rate gradually decreases; this is known as stress relaxation. The most commonly recycled viscoelastic representation is the higher-convected Maxwell fluid model. In recent years, researchers have focused on the flow and heat transfer properties of Maxwell fluids via the efficacy of polymers with low molecular weight. Tan and Xu [1]

CONTACT Pallamkuppam Vinodh Kumar  pallamkuppamvinodhkumar@gmail.com

studied the viscoelastic behavior of the fluid under no-slip conditions using the Maxwell fluid concept. The precise answer was obtained using discrete inverse transform.

Jamil and Fetecau [2] used the Maxwell liquid to calculate helical flows. The imposed shear force produced the flow at the plate in this case. The action of magnetite nanofluid across a spinning disc with an exterior magnetic field is elucidated by Kumar et al. [3]. Khan et al. [4] studied Maxwell fluid boundary layer flow around a stretchable horizontal rotational cylinder among a transverse magnetic field. Kumar et al. [5] assessed the effects of thermophoretic molecule displacement and magnetic dipole on Maxwell liquid flow over a stretched sheet. Loenko et al. [6] explored non-Newtonian natural convection with sinusoidal wall temperature dependency. Saif et al. [7] studied analytical modeling for melting cylindrical planes in upper-convected Maxwell fluid. Zhang et al. [8] investigated a Maxwell-power-law fluid's flow and heat transfer characteristics through variable thickness limited by an unstable stretched sheet. Cheng et al. [9] considered the flow properties of an elastoviscoplastic non-Newtonian fluid comprising hybrid nanostructures and grime molecules, as well as heat transfer treatment. Using a finite-volume approach, Pimenta and Alves [10] examined the coupled heat transmission properties in the unconstrained stream of a viscoelastic fluid through a sphere. Dong et al. [11] investigated the relationship between non-Newtonian flow and one-dimensional non-Fourier heat transference in nanosystems.

Homogeneous reactions originate in most fluid (homogeneous), whereas heterogeneous reactions originate in select catalytic planes. Catalysis, biology, and emission all use homogeneous and heterogeneous processes. An intricate relationship exists among homogeneous and heterogeneous reactions involving simultaneous synthesis and dissipation of reactant species in the fluid than on the catalytic planes. Chaudhary and Merkin [12] investigated boundary layer flow dynamics. In another study, Merkin [13] used heterogeneous and homogeneous procedures to flow of viscous liquid on the stretchy plane and he studied homogeneous reaction and the first-order heterogeneous reaction utilizing cubic autocatalysis. Venkata Subba Rao et al. [14] studied mass and heat transport in a perpendicular permeable cone immersed in a permeable channel through a chemical reaction. According to Ayub et al. [15], a three-dimensional liquid hybrid nanofluid with an angled magnetic plane significantly affects homogeneous and heterogeneous processes. Khan et al. [16] addressed the unsteady MHD Maxwell fluid flow for heterogeneous responses on rotating and vertically moving discs. Mishra et al. [17] investigated the chemical processes that cause heat generation or absorption in a micropolar nanofluid moving across a non-linear stretched plane. Sheikh et al. [18] studied the non-linear Rosseland approximation for Newtonian fluid boundary layer flow with unequal chemically reactive species diffusivities. Ali et al. [19] studied three-dimensional Cross fluid fluxes.

The research has advanced to include rotating disc-generated flows in a variety of functional sectors, such as gas turbine technology, centrifugal thrusts, rotor-stator devices, rotary air filters, and chemical engineering. Von Kármán describes an incompressible liquid orbiting a rotating disc [20]. A radial pressure gradient regulates the centrifugal forces. Instead, an axial flow towards the disc replaces it. Von Kármán [20] utilized an integral approximation method to get analytic answers. Cochran [21] computed a few von Kármán errors and approximated the governing equations of motion numerically. Stuart [22] studied laminar flow suction near a spinning porous disc. To address this problem, Ackroyd [23] employed exponential formulas with negative exponents. If an incompressible fluid spins

a stationary disc, it creates a dual problem. Bödewadt [24] was the first to use boundary layer calculations to investigate this problem. He noticed that the radially inner fluid motion towards a disc through accomplish the mass conservation requirement, balanced by an axial flow upwards. Owens and Rogers [25] published a monograph that reviewed the research on rotating disc-induced flow problems from 1989. Turkiymazoglu [26] considered the flow regime of an electrically charged Maxwell fluid over a radially flexible disc. Khan et al. [27] studied radiative von Kármán whirling flow generated by a spinning disc. Yao et al. [28] studied the rheological properties of von Kármán whirling flow heat transfer enhancement through elastic instability. Hafeez and Khan [29] demonstrated the Cattaneo-Christov mass flux and heat concepts in the flow of Oldroyd-B liquid across the revolving disc with a chemical reaction. Shehzad et al. [30] explored the numerical fluid solution flow owing to spinning disc uphill and downhill motion.

Thermal radiation is the dispersion of electromagnetic radiation from a heated plane in all directions. Thermal radiation has a significant influence on high-temperature processes and space technology. The use of thermal radiations mainly controls the heat transfer process in the polymer manufacturing industry. Thermal radiations are essential on the plane due to the heat transfer coefficient. The entropy reduction of a radiative pair stress fluid flowing across a permeable elongated cylinder with thermal conductivity is investigated by Gangadhar et al. [31]. Anwar et al. [32] investigated the effects of thermal energy on a changeable velocity and temperature Brinkman-type ferrofluid. Thriveni and Mahanthesh [33] developed a computational method for the flow and heat transport mechanisms in an annulus loaded with hybridized nano liquid with quadratic heat radiation and convection. Shafiq et al. [34] examined the influence of dual lamination on the stagnation point of a radiative Walter's B nano liquid being pushed over the Riga plane. Mackolil and Mahanthesh [35] studied the impact of heat radiation on nanoliquid owing to thermal Marangoni convection. Increasing the radiated heat variable raises the temperature and density of the thermal perimeter, according to Zhang et al. [36]. Khan and Nadeem [37] explored a three-dimensional Maxwell fluid flow across a perpendicular plane. References [38–47] are mainly devoted to linear and non-linear thermal radiations in heat transfer research.

According to one study, the non-Newtonian rotating disc problem has gotten minimal attention. There is no attempt to investigate the non-Newtonian Maxwell fluid over the spinning disc along the heat source. The classical von Karman viscous pump problem will be generalized to the situation where the rotating disk is permitted to stretch in the radial direction. The Maxwell fluid flow sequence is explored for heat and mass transmission characteristics as well as homogeneous-heterogeneous responses. Non-linear thermal radiation and Joule heating those are used to improve the heat transmission. Based on flow similarities, the controlling PDEs become a bent of conventional non-linear differential equations. These ODEs for flow and energy transfer are solved using MATLAB's built-in numerical technique, bvp4c. In the end, the consequences of this physical issue are visually explained.

2. Mathematical formulation

Assume a three-dimensional Maxwell fluid flow in the axial path of a spinning stretchy disc subjected to a constant magnetic field B_0 . When minor magnetic Reynolds numbers

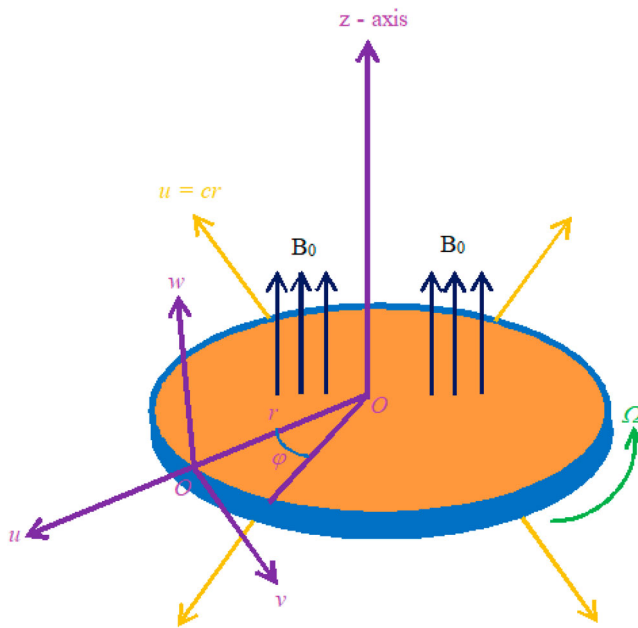


Figure 1. Flow of schematic diagram.

are considered, the induced magnetic field can be ignored. The heat transfer characteristics of the system are also described by the non-linear radiative heat flow. The energy equation also takes into account viscous dissipation and Joule heating. The cylindrical coordinate system is considered in order to better understand a physical model, as illustrated in Figure 1.

The homogeneous-heterogeneous reactions in boundary layer flow and catalytic plane prompted Chaudhary and Merkin [12]. The Cubic autocatalysis homogenous reaction is



For isothermal reaction



In which A and B represent chemical species, a and b represent the concentrations, and k_c and k_s represent the rate constants. The isothermal nature of the reactions tends to suggest that they are taking place. [Khan et al. [27]] governed the Maxwell three-dimensional flow along a magnetic field.

$$\Delta \cdot \vec{\mathbf{V}}_1 = 0, \quad (3)$$

$$\rho_f (\vec{\mathbf{V}}_1 \cdot \nabla) \vec{\mathbf{V}}_1 = -\nabla P + \nabla S + J \times B, \quad (4)$$

$$(\rho c_p)_f (\vec{\mathbf{V}}_1 \cdot \nabla) T = k \nabla^2 T - \frac{\partial q_{rad}}{\partial z} + \mu \psi + \frac{J^2}{\sigma^*} + Q_0(T - T_\infty), \quad (5)$$

$$(\vec{\mathbf{V}}_1 \cdot \nabla) a = D_A \nabla^2 a - k_c ab^2, \quad (6)$$

$$(\vec{\mathbf{V}}_1 \cdot \nabla) b = D_B \nabla^2 b - k_c ab^2. \quad (7)$$

Where \vec{V}_1 is the velocity vector, \mathbf{S} represents the additional stress tensor for the non-Newtonian fluid as

$$\mathbf{S} + \lambda_1 \frac{D\mathbf{S}}{Dt} = \mu A_1. \quad (8)$$

In which A_1 is the primary Rivlin Erickson tensor written as

$$A_1 = (\nabla \cdot \vec{V}_1) + (\nabla \cdot \vec{V}_1)^T.$$

λ_1 represents the relaxation-time parameter whereas $\frac{D}{Dt}$ represents the upper-convected derivative. The given equations are valid for a tensor of second rank \mathbf{S} .

$$\frac{D\mathbf{S}}{Dt} = \frac{\partial \mathbf{S}}{\partial t} + (\vec{V}_1 \cdot \nabla) \mathbf{S} - L\mathbf{S} - \mathbf{S}L^T. \quad (9)$$

In which $L = grad \vec{V}_1$ and in the Equation (4), $\vec{V}_1 = [u_1(r, z), v_1(r, z), w_1(r, z)]$ represents the velocity vector among constituents with it radial-, azimuthal-, and axial – directions. Further, $J = \sigma^*(\vec{V}_1 \times B)$ represents the electric current density and σ^* represents the electrical conductivity of the base fluid, P represents the liquid pressure, $B = [0, 0, B_0]$ represents the magnetic field strength, ρ_f represents the liquid density, L is the characteristic length and k represents as thermal conductivity of the fluid.

Assuming that the equations (8) and (9) and relating the boundary layer calculations, the governing continuity, momentum, energy, and concentration equations will be

$$\begin{aligned} \frac{\partial u_1}{\partial r} + \frac{u_1}{r} + \frac{\partial w_1}{\partial z} &= 0, \quad (10) \\ u_1 \frac{\partial u_1}{\partial r} + w_1 \frac{\partial u_1}{\partial z} - \frac{v_1^2}{r} &= v \frac{\partial^2 u_1}{\partial r^2} \\ &- \lambda_1 \left(u_1^2 \frac{\partial^2 u_1}{\partial r^2} + w_1^2 \frac{\partial^2 u_1}{\partial z^2} + 2u_1 w_1 \frac{\partial^2 u_1}{\partial r \partial z} - \frac{2u_1 v_1}{r} \frac{\partial v_1}{\partial r} \right) \\ &- \frac{\sigma B_0^2}{\rho_f} \left(u_1 + w_1 \lambda_1 \frac{\partial u_1}{\partial z} \right), \quad (11) \end{aligned}$$

$$\begin{aligned} u_1 \frac{\partial v_1}{\partial r} + w_1 \frac{\partial v_1}{\partial z} + \frac{u_1 v_1}{r} &= v \frac{\partial^2 v_1}{\partial r^2} \\ &- \lambda_1 \left(u_1^2 \frac{\partial^2 v_1}{\partial r^2} + w_1^2 \frac{\partial^2 v_1}{\partial z^2} + 2u_1 w_1 \frac{\partial^2 v_1}{\partial r \partial z} + \frac{2u_1 v_1}{r} \frac{\partial u_1}{\partial r} \right) \\ &- \frac{\sigma B_0^2}{\rho_f} \left(v_1 + w_1 \lambda_1 \frac{\partial v_1}{\partial z} \right), \quad (12) \end{aligned}$$

$$\begin{aligned} u_1 \frac{\partial T}{\partial r} + w_1 \frac{\partial T}{\partial z} &= \alpha \left(\frac{\partial^2 T}{\partial z^2} \right) - \frac{1}{(\rho c_p)_f} \frac{\partial q_{rad}}{\partial z} + \frac{\sigma}{(\rho c_p)_f} B_0^2 (u_1^2 + v_1^2) \\ &+ \frac{\mu_f}{(\rho c_p)_f} \left[\left(\frac{\partial u_1}{\partial z} \right)^2 + \left(\frac{\partial v_1}{\partial z} \right)^2 \right] + \frac{Q_0}{(\rho c_p)_f} (T - T_\infty), \quad (13) \end{aligned}$$

$$u_1 \frac{\partial a}{\partial r} + w_1 \frac{\partial a}{\partial z} = D_A \left(\frac{\partial^2 a}{\partial z^2} \right) - k_c a b^2, \quad (14)$$

$$u_1 \frac{\partial b}{\partial r} + w_1 \frac{\partial b}{\partial z} = D_B \left(\frac{\partial^2 a}{\partial z^2} \right) + k_c a b^2. \quad (15)$$

Here D_A and D_B represent the diffusion coefficients, α represents the thermal diffusivity, and T represents the fluid temperature. With the integration of the Rosseland similarity, of ensuing radiative heat flux is

$$q_{rad} = -\frac{4\hat{\sigma}}{3k^*} \frac{\partial T^4}{\partial z}, \quad (16)$$

where k^* represents the mean absorption coefficient and $\hat{\sigma}$ represents the Stefan-Boltzmann constant. Suppose the temperature variations in the flow are much more minor than they are. Consequently, mentioning T^4 in the Taylor series about T_∞ and excluding the terms for higher order given as

$$q_{rad} = -\frac{16\hat{\sigma}T^3}{3k^*} \frac{\partial T}{\partial z}. \quad (17)$$

Considering the Equation (17), and energy equation (13) forms into

$$\begin{aligned} u_1 \frac{\partial T}{\partial r} + w_1 \frac{\partial T}{\partial z} = & \alpha \left(\frac{\partial^2 T}{\partial z^2} \right) + \frac{16\hat{\sigma}}{3k^*(\rho c_p)_f} \frac{\partial}{\partial z} \left(T^3 \frac{\partial T}{\partial z} \right) + \frac{\sigma}{(\rho c_p)_f} B_0^2 (u_1^2 + v_1^2) \\ & + \frac{\mu_f}{(\rho c_p)_f} \left[\left(\frac{\partial u_1}{\partial z} \right)^2 + \left(\frac{\partial v_1}{\partial z} \right)^2 \right] + \frac{Q_0}{(\rho c_p)_f} (T - T_\infty), \end{aligned} \quad (18)$$

with boundary conditions

$$u_1 = U_w = cr, \quad v_1 = \Omega r, \quad w_1 = 0, \quad T = T_w, \quad D_A \frac{\partial a}{\partial z} = k_s a, \quad D_B \frac{\partial b}{\partial z} = -k_s a, \quad \text{at } z = 0, \quad (19)$$

$$u_1 = 0, \quad v_1 = 0, \quad T \rightarrow T_\infty, \quad a \rightarrow a_0, \quad b \rightarrow 0, \quad \text{as } z \rightarrow \infty. \quad (20)$$

Here c represents the stretching rate, a_0 represents the positive dimensional constant and Ω represents as swirl rate, The given below are the similarity variables:

$$\begin{aligned} u_1 = crF, \quad v_1 = crG, \quad w_1 = \sqrt{cv}H, \quad \eta = \sqrt{\frac{c}{v}}z, \\ \theta(\eta) = \frac{T - T_\infty}{T_w - T_\infty}, \quad \frac{a}{a_0} = g(\eta), \quad \frac{b}{a_0} = h(\eta). \end{aligned} \quad (21)$$

The dimensionless radial-, azimuthal-, and axial-velocity components are $F(\eta)$, $G(\eta)$ and $H(\eta)$, correspondingly, the dimensionless temperature is $\theta(\eta)$, the dimensionless concentration of homogeneous bulk fluid is $g(\eta)$, and the dimensionless concentration of heterogeneous catalyst at the plane is $h(\eta)$. With these affinity transformations, Equations (10)–(12), (14), (15), (18) and (19) turn into the dimensionless model given below:

$$H' + 2F = 0, \quad (22)$$

$$F'' - F^2 + G^2 - HF' - \beta_1(H^2F'' + 2FF'H - 2HGG') - M(F + \beta_1HF') = 0, \quad (23)$$

$$G'' - 2FG - HG' - \beta_1(H^2G'' + 2FG'H + 2HGF') - M(G + \beta_1HG') = 0, \quad (24)$$

$$\left(1 + \frac{4}{3}Rd\right)\theta'' + \frac{3}{4}Rd \left(\begin{array}{l} (\theta_w - 1)^3(3\theta^2\theta'^2 + \theta^3\theta'') + 3(\theta_w - 1)^2(2\theta\theta'^2 + \theta^2\theta'') \\ + 3(\theta_w - 1)(\theta'^2 + \theta\theta'') \end{array} \right) - Pr\theta'H + Ec(F^2 + G^2) + EcM(F^2 + G^2) + PrQ\theta = 0, \quad (25)$$

$$\frac{1}{Sc}g'' - Hg' - k_1gh^2 = 0, \quad (26)$$

$$\frac{\delta}{Sc}h'' - Hh' + k_1gh^2 = 0, \quad (27)$$

with

$$\begin{cases} F(0) = 1, G(0) = \omega, H(0) = 0, \theta(0) = 1, g'(0) = k_2g(0), \delta h'(0) = -k_2g(0), \\ F \rightarrow 0, G \rightarrow 0, \theta \rightarrow 0, g \rightarrow 1, h \rightarrow 0, \text{ as } \eta \rightarrow \infty. \end{cases} \quad (28)$$

$\omega = \frac{\Omega}{c}$ represents the rotation strength parameter calculating the proportion of swirl to stretch rates, and $\omega = 0$ infers pure stretching minus rotation. And also, M represents the magnetic field (the hydrodynamic situation is salvaged by substituting $M = 0$), β_1 represents the Deborah number, θ_w represents the temperature ratio parameter, Rd represent the radiation parameter, δ is the ratio of mass diffusion coefficients, Pr represents the Prandtl number, k_1 represents the degree of strength of homogeneous reaction, Sc represents the Schmidt number, k_2 represents the amount of strength of heterogeneous reaction, Ec represents the Eckert number, and Q represents the heat generative or absorptive parameter. The dimensionless quantities are as follows:

$$\begin{aligned} M &= \frac{\sigma B_0^2}{c\rho_f}, \beta_1 = \lambda_1 c, Rd = \frac{4\sigma^* T_\infty^3}{kk^*}, \theta_w = \frac{T_w}{T_\infty}, Pr = \frac{\nu}{\alpha}, \\ k_1 &= \frac{k_c a^2}{c}, Sc = \frac{\nu}{D_A}, k_2 = \frac{k_s}{D_A} \sqrt{\frac{\nu}{c}}, Ec = \frac{U_w^2}{c_p(T_w - T_\infty)}, \\ Q &= \frac{Q_0}{c\nu(\rho c_p)_f}, \delta = \frac{D_B}{D_A}. \end{aligned} \quad (29)$$

The diffusion coefficients of chemical species A and B remains the equivalent scale. This assumption proceeds to research when the diffusion coefficients of D_A and D_B are similar, especially $\delta = 1$ (see Merkin [13]). In fact, this supposition yields

$$g(\eta) + h(\eta) = 1. \quad (30)$$

Thus, Equations (25) and (26) become

$$\frac{1}{Sc}g'' - Hg' - k_1g(1-g)^2 = 0. \quad (31)$$

In circumstances of this case

$$g'(0) = k_2g(0), \quad g(\infty) \rightarrow 1. \quad (32)$$

Notably, when the parameter β_1 is 0, the current Maxwell model issue simplifies to a viscous fluid.

Efficacy in terms of heat transmission:

The local Nusselt number Nu_r maybe used to evaluate the convective thermal conductivity over the disk plane. The Nusselt number Nu_r is defined by the Fourier law, which is applied to physical data. The following is the mathematical representation for the quantity:

$$Nu_r = \frac{rq_w}{k(T_w - T_\infty)}, \quad (33)$$

with $q_w = -k \left(1 + \frac{16\sigma^* T^3}{3kk^*} \right) \left(\frac{\partial T}{\partial z} \right)_{z=0}$.

Non-dimensionally, it is

$$Re^{-1/2} Nu_r = - \left(1 + \frac{4}{3} Rd(1 + (\theta_w - 1)\theta(0))^3 \theta'(0) \right), \quad (34)$$

where $Re = \frac{rU_w}{\nu}$ represents the local Reynolds number.

3. Numerical solution

The nonlinear system ODEs (22)–(25), (31) is modified into a first-order differential equation with boundary conditions (28) and (32). Now, the `bvp4c` technique is applied to determine the first-order ODEs. For this proposes, the procedure of transformed ODEs is followed as:

$$\begin{aligned} \Psi_1 &= H, \Psi'_1 = H', \Psi_2 = F, \Psi_3 = F', \Psi'_3 = F'', \Psi_4 = G, \\ \Psi_5 &= G', \Psi'_5 = G'', \Psi_6 = \theta, \Psi_7 = \theta', \Psi'_7 = \theta'', \\ \Psi_8 &= g, \Psi_9 = g', \Psi'_9 = g'', \end{aligned} \quad (35)$$

where

$$\Psi'_1 = -2\Psi_2, \quad (36)$$

$$\Psi'_3 = \frac{1}{(1 - \beta_1 \Psi_1^2)} \left[\Psi_2^2 - \Psi_4^2 + \Psi_1 \Psi_3 + \beta_1(2\Psi_2 \Psi_3 \Psi_1 - 2\Psi_1 \Psi_4 \Psi_5) \right], \quad (37)$$

$$\Psi'_5 = \frac{1}{(1 - \beta_1 \Psi_1^2)} \left[2\Psi_2 \Psi_4 + \Psi_1 \Psi_5 + \beta_1(2\Psi_2 \Psi_5 \Psi_1 + 2\Psi_1 \Psi_4 \Psi_3) \right], \quad (38)$$

$$\begin{aligned} \Psi'_7 &= \left(\frac{3}{3 + 4Rd + 4Rd((\theta_w - 1)^3 \Psi_6^3 + 9(\theta_w - 1)^2 \Psi_6^2 + 9(\theta_w - 1) \Psi_6)} \right) \\ &\times \left(Pr \Psi_1 \Psi_7 - 4Rd(\theta_w - 1)^3 \Psi_6^2 \Psi_7^2 - 8Rd(\theta_w - 1)^2 \Psi_6 \Psi_7^2 - 4Rd(\theta_w - 1) \Psi_7^2 \right. \\ &\left. - Ec(\Psi_3^2 + \Psi_5^2) - EcM(\Psi_2^2 + \Psi_4^2) - Pr Q \Psi_6 \right), \end{aligned} \quad (39)$$

$$\Psi'_9 = Sc(\Psi_1 \Psi_9 + k_1(1 - \Psi_8)^2), \quad (40)$$

with boundary condition

$$\begin{aligned} \Psi_2(0) &= 1, \Psi_1(0) = 0, \Psi_6(0) = 1, \Psi_9(0) = k_2 \Psi_8(0), \\ \Psi_2 &\rightarrow 0, \Psi_4 \rightarrow 0, \Psi_6 \rightarrow 0, \Psi_8 \rightarrow 1, \text{ as } \eta \rightarrow \infty. \end{aligned} \quad (41)$$

In the numerical procedure scheme we choose Matlab software which satisfies our desired `bvp4c` methodology in conjunction with shooting criteria. The inner iteration is executed with convergence criteria of 10^{-6} in all cases taking step size $\Delta = 0.01$.

3.1. Code of authentication

With the assumption that $\beta_1 = 0.0, Rd = 0.0, Ec = 0.0, Q = 0.0$, we computed the numbers of $F'(0)$ and $G'(0)$ for several values of M and ω to guarantee the correctness of our research. These values are given in Table 1 and matched to Turkylmazoglu [26]. Additionally, we calculated the values of $-H(\infty)$ and $-\theta'(0)$ for different values of M and ω by assuming that $\beta_1 = 0.0, Rd = 0.0, Ec = 0.0, Q = 0.0$. Table 2 includes these values and correlates them to those reported by Khan et al. [27]. It substantiates the intended precision. Accordingly, the verification code is validated.

4. Statistical scheme

The different consequences of linked factors for the flow profile are now being discussed. However, before proceeding, it is vital to understand the underlying relationship between physical properties, which we shall demonstrate in Table 3 by presenting the local Nusselt value. The values of the correlation coefficients are then calculated and displayed in Table 4.

4.1. On possible error

Using the potential error is a simple and popular method to validate the observed correlation coefficient. Fisher [48] came up with several ground-breaking ideas. The relationships

Table 1. Assessment of $F'(0)$ and $G'(0)$ for varied values of M and ω .

M	ω	Turkylmazoglu [26]		Present outcomes	
		$F'(0)$	$G'(0)$	$F'(0)$	$G'(0)$
0	0	-1.173720738	0.000000000	-1.173720739	-0.000000000
	1	-0.948313756	1.486952682	-0.948313756	1.486952682
	2	-0.326243978	3.127828177	-0.326243978	3.127828178
	5	3.193732989	9.253541181	3.193732989	9.253541181
	10	12.7208997661	22.913407256	12.720899766	22.913407257
2	0	40.9056723025	60.012930540	40.905672303	60.012930540
	1	-1.830489674	0.000000000	-1.830489675	-0.000000000
	2	-1.663452548	2.023944904	-1.663452549	2.023944904
	5	-1.175347018	4.113493830	-1.175347018	4.113493830
	10	1.8929454707	11.140599491	1.892945471	11.140599491
20	0	10.8333844902	25.722555162	10.833384490	25.722555162
	1	38.1879775732	64.060450067	38.187977573	64.060450067

Table 2. Assessment of $-H(\infty)$ and $-\theta'(0)$ for varied values of M and ω .

M	ω	Khan et al. [27]		Present outcomes	
		$-H(\infty)$	$-\theta'(0)$	$-H(\infty)$	$-\theta'(0)$
0	0	1.502 952 500	0.851 993 748 0	1.502987172	0.851991421
	1	1.573 049 479	0.875 663 350 0	1.573072470	0.875662140
	2	1.728 816 732	0.930 411 517 8	1.728825287	0.930411191
	5	2.252 086 675	1.129 140 496 0	2.252086886	1.129140493
	10	1.038 474 351	0.726 188 988 0	1.038474413	0.726086563
2	0	1.074 894 568	0.742 289 416 0	1.074894629	0.742212296
	1	1.173 952 446	0.785 400 968 0	1.173952489	0.785365438
	2	1.640 958 240	0.980 286 049 0	1.640958246	0.980285183

Table 3. Values of Nu_r for varied values of relevant boundaries.

Rd	θ_w	Pr	Ec	$Re^{-1/2}Nu_r$	
				$M = 0$	$M = 0.5$
0.1	1.2	7	0.2	3.969675550	2.135746821
0.2				3.894695657	2.161380480
0.3				3.820947970	2.176589163
0.4				3.748907315	2.183789486
0.5				3.678845501	2.184784583
	1.4			4.349199040	2.571549526
	1.6			4.750547616	2.958290744
	1.8			5.123162171	3.271696254
	2.0			5.432812221	3.491755252
		1		-1.190118237	-3.256690237
		3		1.240343294	-0.719357141
		5		2.775176931	0.887685156
		7		3.969675550	2.135746821
			-0.4	10.840702012	14.027762501
			-0.2	8.568112340	10.100244541
			0.0	6.277749936	6.136212348
			0.2	3.969675550	2.135746821
			0.4	1.643840986	-1.901465441

Table 4. Values of the correlation coefficient.

r	$Re^{-1/2}Nu_r$	
	$M = 0$	$M = 0.5$
Rd	-0.9999096	0.927397
θ_w	0.9989971	0.992191
Pr	0.986551	0.986619
Ec	-0.9999896	-0.99999

shown below describe the kinds of errors that could arise.

$$P.E(r) = 0.6745 \frac{(1 - r^2)}{\sqrt{n}}, \quad (42)$$

The r represents as correlation coefficient, and n represents the number of observations or figures obtained in each situation of computing Nu_r irrespective of the occurrence and absence of magnetic field and the prominence of the factor 0.6745 is that $\mu \pm 0.6745\sigma$ comprises half of the area in a normal distribution. Here μ represents the mean, and σ represents the standard deviation of the sample. The following is the rule that will be used to make the ultimate decision:

$$\left. \begin{aligned} r < P.E(r) &\Rightarrow \text{correlation is not significant} \\ r > P.E(r) &\Rightarrow \text{correlation is significant} \end{aligned} \right\} \quad (43)$$

4.2. Statistical declaration about parameters

For calculating the correlation coefficient, researchers apply Pearson's correlation coefficient, indicated as r . Pearson's correlation coefficient is used chiefly for grouping. The method entails determining the sample's covariance and variance. Assume two datasets $\{x_1, x_2, \dots, x_k\}$ and $\{y_1, y_2, \dots, y_k\}$ and the formula stands $r = \frac{\sum_{i=1}^k (x_i - \bar{x})(y_i - \bar{y})}{\sqrt{\sum_{i=1}^k (x_i - \bar{x})^2} \sqrt{\sum_{i=1}^k (y_i - \bar{y})^2}}$ where

Table 5. Values of $P.E(r)$.

$P.E(r)$	$Re^{-1/2}Nu_r$	
	$M = 0$	$M = 0.5$
Rd	0.0000546	0.042211
θ_w	0.000605	0.004693
Pr	0.00901	0.008965
Ec	0.00000629	0.00000889

Table 6. Values of $\frac{r}{P.E(r)}$.

$\frac{r}{P.E(r)}$	$Re^{-1/2}Nu_r$	
	$M = 0$	$M = 0.5$
Rd	-18325.2	21.97062
θ_w	1652.032	211.4254
Pr	109.4922	110.0492
Ec	-159052	-112468

\bar{x}, \bar{y} are the mean sample. Firstly, let us assess it. We got the value of Nu_r in the absence of M for the parameter Rd in Table 3. Taking the Cf_r value in the 5th column (i.e. $M = 0$ column) will be assumed as the 2nd dataset i.e. $\{y_1, y_2, \dots, y_k\}$. Five considerations.

i.e., the value of k is 5 are calculated. We know, $\bar{x} = 0.3$, $\bar{y} = 3.822614$ and $\sum_{i=1}^k (x_i - \bar{x})^2 =$

0.1 , $\sum_{i=1}^k (y_i - \bar{y})^2 = 0.0529254$. Using the same method as before, we can determine the values of r as -0.9999096 in Table 4 by computing the remaining values. Subsequent estimation of the plausible error values in the Table 5 noted $P.E(r) = 0.0000546$ applying the technique as described in (42) in which $r = -0.9999096$ and $n = 5$. Later the modulus of the values $\frac{r}{P.E(r)}$ in the Table 6 was calculated. Following Equation (43), the correlation coefficients are substantial, and parameters strongly correlate to physical properties.

5. Results and discussion

This part of the work provides a framework for understanding flow, temperature, and mass distributions. The magneto Maxwell fluid flow over a stretchy disc is numerically studied. Non-linear thermal radiation and Joule heating are investigated. These responses are based on the concentration of fluid volume. The parametric analysis examines the velocity components $F(\eta)$, $G(\eta)$ and $H(\eta)$, the temperature field $\theta(\eta)$, and the nanoparticle concentration field $g(\eta)$. The effect of limitations, for example, rotation $0.0 \leq \omega \leq 8.0$ and magnetic field $0.0 \leq M \leq 4.0$ are studied as the velocity components $F(\eta)$, $G(\eta)$, $H(\eta)$ And the temperature field $\theta(\eta)$. The impact of Deborah number $0.0 \leq \beta_1 \leq 0.2$ as the velocity constituents $F(\eta)$, $G(\eta)$, $H(\eta)$ are investigated. Likewise of radiation parameter $0.0 \leq Rd \leq 1.6$, the Eckert number $0.0 \leq Ec \leq 1.6$, the heat source parameter $-2.0 \leq Q \leq 1.0$, and the temperature ratio parameter $1.4 \leq \theta_w \leq 2.2$ on the temperature distribution $\theta(\eta)$ are also examined. The impacts of the homogeneous reaction strength $0.1 \leq k_1 \leq 0.7$, the heterogeneous (plane) reaction strength parameter $0.2 \leq k_2 \leq 1.0$, the magnetic field $0.0 \leq M \leq 4.0$ and the Schmidt number $0.32 \leq Sc \leq 2.62$ on the volume concentration

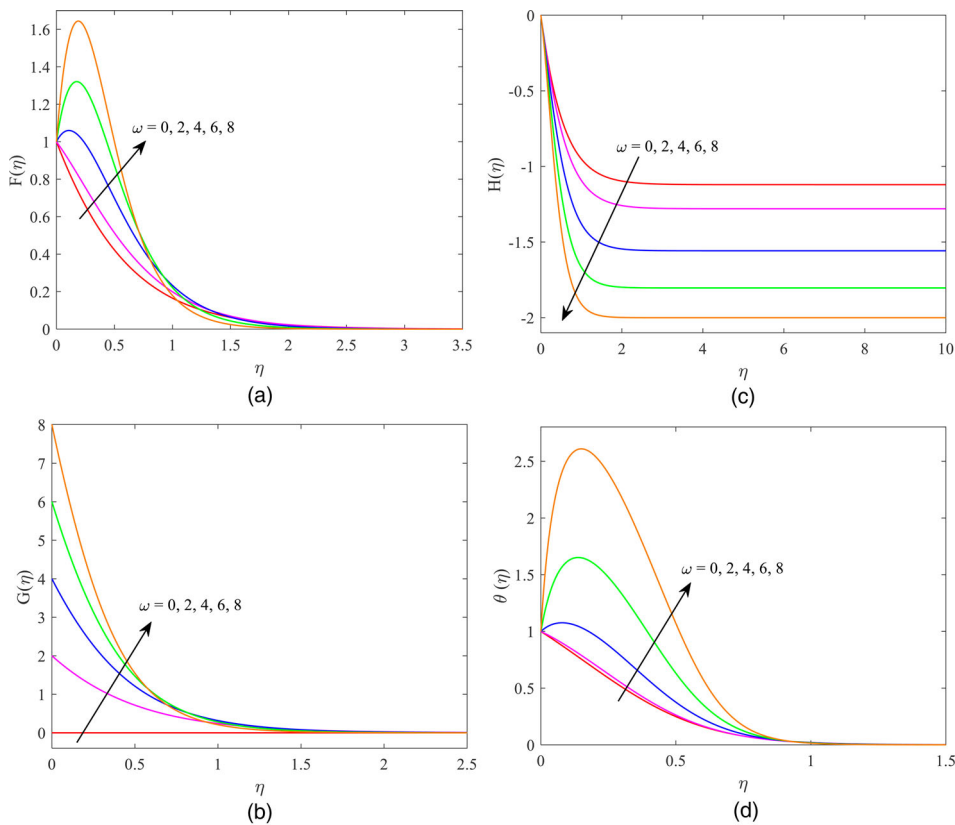


Figure 2. (a) Impact of ω on radial velocity. (b) Impact of ω on azimuthal velocity. (c) Impact of ω on tangential velocity. (d) Impact of ω on temperature.

$g(\eta)$ are considered. The entire presentation is accomplished by including the values of the parameter as $Pr = 7.0, M = 1.0, \beta_1 = 0.1, \omega = 3.0, Rd = 0.1, Ec = 0.2, Q = 0.1, \theta_w = 1.2, Sc = 0.22, k_1 = 0.1$ and $k_2 = 0.1$ unless otherwise specified.

Axial, azimuthal, and radial velocity patterns and temperature profiles from are Figure 2(a-d) for given values of those physical constraints. As seen in Figure 2a, the radial velocity rises with and eventually surpasses the stretching velocity. That the rotation speed increases, the fluid particles are accelerated in a circular direction by centrifugal force, exceeding the stretching number. However, as one moves away from the disc, the radial velocity decreases. It means that in the disc plane, the centrifugal force has a limited influence. The natural rise in angular velocity toward the disk's plane is shown in Figure 2b. Axial velocity falls as rotation increases, owing to more pumping of fluid particles pushed to the wall by negative axial stretching (Figure 2c). Furthermore, when the rotational velocity increases, the fluid temperature drops due to dissipation and Joule heating, resulting in heat loss and a reduction in stretching, which will be essential as the system cools.

Figure 3 (a-d) illustrates the impact on a magnetic field on velocity and temperature profiles. The velocity profiles in all directions drastically drop as the magnetic field strength increases. The results are physically valid, since higher values of the magnetic parameter M

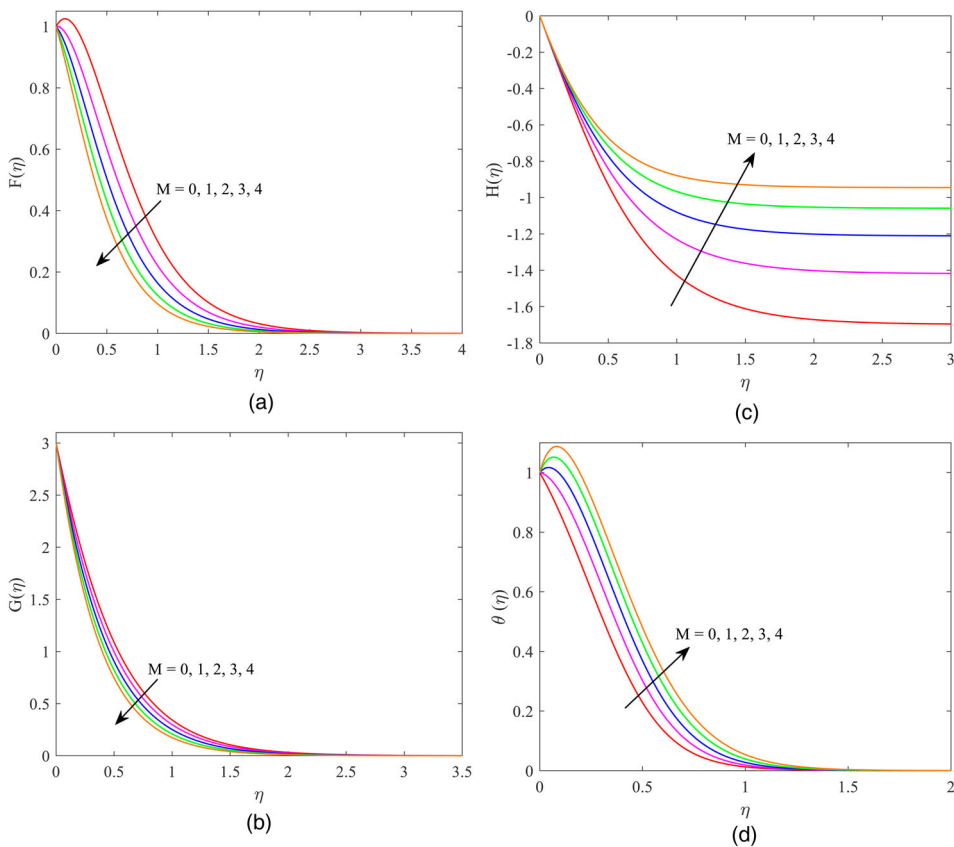


Figure 3. (a) Impact of M on radial velocity. (b) Impact of M on azimuthal velocity. (c) Impact of M on tangential velocity. (d) Impact of M on temperature.

boost up the Lorentz force that occurs in the fluid flow due to the transverse applied magnetic field and provides the resistance to the flow velocity. Hence, in the results, the velocity of fluid decreases. The temperature profile rises due to increased skin friction and offers significant friction to flowing fluid, in contrast to the velocity field. The vertical magnetic field heats the fluid. A perpendicular magnetic field is utilized to an electrically charged fluid to generate the Lorentz force, reducing the disk's flow while raising its temperature. As M raises, the radial, tangential, and axial velocity profiles drop, and the temperature profiles improve, as illustrated in Figure 3(a-d). Thus, as shown in the Figures 2 and 3, the unavoidable heating caused by the magnetic field may be avoided by radial extending the disk. Furthermore, as shown in (Fang [49]), when the disk rotation parameter is exceptionally high, the flow is comparable to that of a von Karman viscous pump. It is valid for the MHD flow calculated.

The velocity fields for greater values of the Maxwell parameter β_1 are shown in Figures 4(a-c). According to the expectations, the results indicate that the radial and azimuthal velocity profiles decrease while the axial velocity profile increases. Increased Maxwell parameter β_1 values in the viscoelastic fluid cause the stress relaxation phenomenon to be more apparent, and the fluid seems to become more solid as the fluid flow rate lowers.

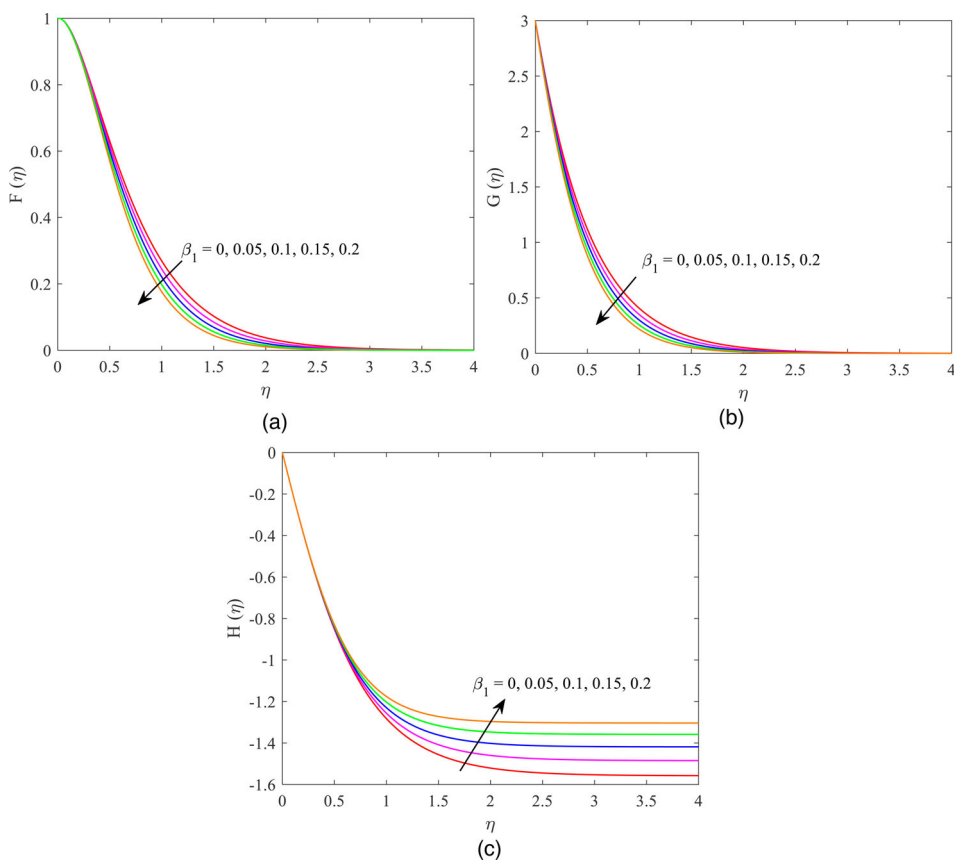


Figure 4. (a) Impact of β_1 on radial velocity. (b) Impact of β_1 on azimuthal velocity. (c) Impact of β_1 on tangential velocity.

With magnetic fields, Figure 5, the Eckert number Ec and radiation parameter Rd affect temperature distribution. When viscous dissipation is permitted, the temperature rises (and falls nearly symmetrically with Ec), increasing the density of thermal boundary layers. In addition to absorbing energy from motion, viscous dissipation converts it into entropy, raising the temperature. In condition $Ec = 0$, viscous and Joule heating is ignored. Mahanthesh et al. [50] made similar findings. This graphic also shows that temperature rises with Rd and the resulting boundary layer density. Because increasing the radiation parameter heats the fluid, increasing the thermal boundary layer density and temperature -this action matched Khan et al. [27].

The combined effect of the temperature ratio and the heat source or sink characteristics on the temperature field is depicted in Figure 6. The fluid temperature is raised due to a heat source component delivering a large amount of heat into the fluid. With more extensive estimations of the temperature ratio and heat source parameters, the temperature distribution also rises Figure 7.

The homogeneous reaction intensity k_1 and the heterogeneous (plane) reaction intensity k_2 are both dependent on the fluid concentration $g(\eta)$. If either k_1 or k_2 are strengthened, the concentration profile becomes narrower, and the resulting concentration boundary layer density becomes thinner. The reason for this is that increasing any of

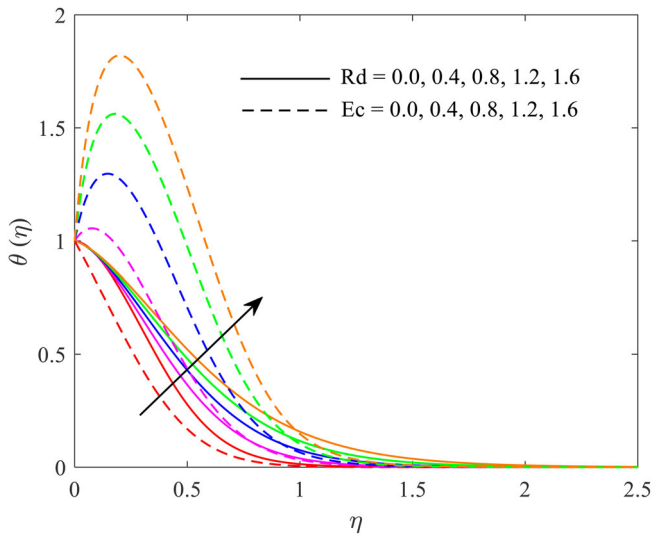


Figure 5. Impact of Rd and Ec on temperature.

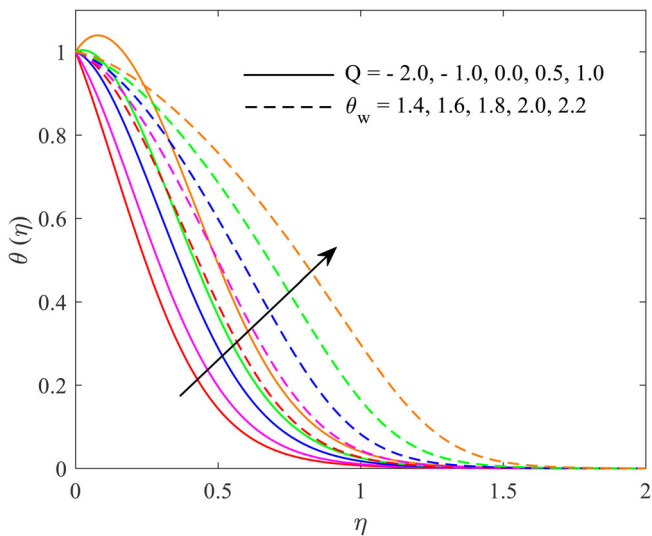


Figure 6. Impact of Q and θ_w on temperature.

these reactions increases the concentration of molecules in the moving fluid, resulting in a drop in the volume concentration $g(\eta)$. If neither of these reactions is strengthened, then the concentration boundary layer thickness becomes thinner. The Schmidt number Sc has been the viscosity/mass diffusivity ratio. Figure 8 illustrates concentration profile graphs for various Schmidt number Sc and magnetic parameter M values. A rise in the Schmidt number reduces mass diffusivity, which raises fluid concentration, as expected. Furthermore, increasing the magnetic field strength decreases the concentration profile induced by the resistive force generated by magnetic force, such as the Lorentz force.

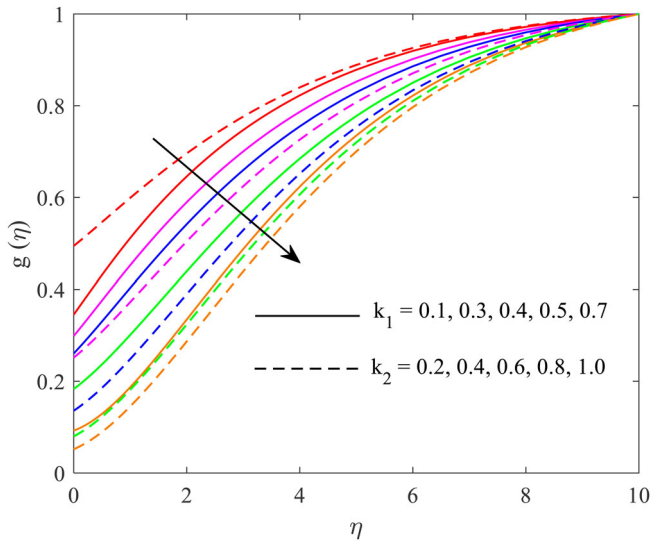


Figure 7. Impact of k_1 and k_2 on concentration.

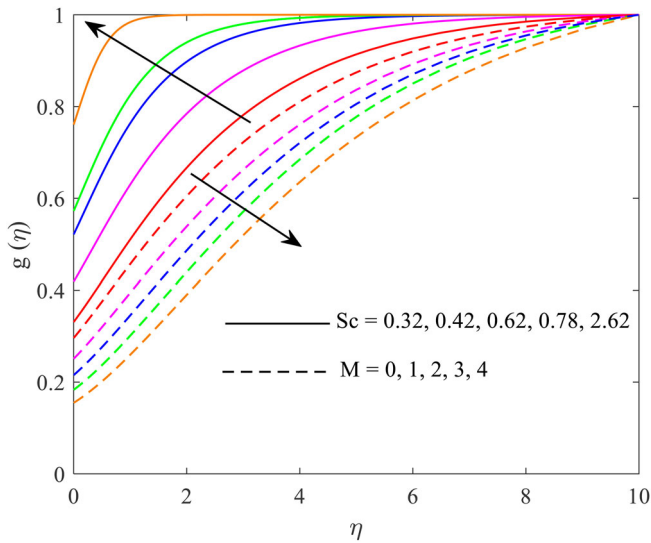


Figure 8. Impact of Sc and M on concentration.

The mathematical calculations in the local Nusselt number Nu_r is comprised in the Table 3 for both $M = 0$ and $M = 0.5$. It is noted that when physical factors including the Prandtl number $1.0 \leq Pr \leq 7.0$ rise, the heat rate indicated by the equation $-(1 + Rd(1 + (\theta_w - 1)\theta(0))^3\theta'(0))$ increases, and the temperature ratio $1.4 \leq \theta_w \leq 2.0$. A decreasing trend is perceived for the radiation parameter $0.1 \leq Rd \leq 0.5$ and the Eckert number $-0.4 \leq Ec \leq 0.4$.

6. Conclusion

In the implement of non-linear thermal radiation and homogeneous-heterogeneous processes on the Maxwell magnetofluid circulation across an infinitely flexible spinning disc with a heat source or sink and Joule heating is investigated by this analysis. The non-linear momentum, energy, and concentration calculations were transformed into non – dimensional versions and, after that, numerically solved. Graphs, tables, and a statistical method have been used to illustrate the effect of different relevant factors on the flow system. Grounded on the fundamental research, the researcher had drawn the following significant findings:

- (1) The centrifugal force significantly affects the disc's region, accelerating disc rotation and increasing the radial and azimuthal velocity components while decreasing the axial velocity component.
- (2) The magnetic field aims to slow down the three velocity components in the required direction, leading to a rise in fluid temperature.
- (3) The radiation and heat production parameters substantially enhance the thickness of the thermal barrier layer.
- (4) When compared to just viscous dissipation, it is discovered that Joule heating improves the temperature distribution along the wall.
- (5) When the rotation factor is increased in the magnetic field, all physical variables, notably heat transfer, increase with tangential shear stress and rotational torque increasing more significantly.
- (6) The concentration boundary layer density is a lower limit for the homogeneous and heterogeneous limitations.
- (7) Radiation and the Eckert number increase temperature transmission coefficient at the disc plane while Prandtl and temperature ratio decrease.
- (8) Analytical methods have proven the reality about strongly linked physical attributes.
- (9) The rise in the Schmidt number results in a substantial rise in the concentration profile.

The current study focuses on non-Newtonian fluid steady-state flow. More research on time-dependent flows, within a relevant to rotating hybrid membrane oxygenator systems, could lead to future studies.

Acknowledgements

We are very grateful for the editor and reviewers for their constructive suggestions.

Author contributions

KG and REN modeled the problem and determined. TK wrote the paper. AJC provided useful comments. All the authors read and accepted the final manuscript.

Disclosure statement

No potential conflict of interest was reported by the author(s).

ORCID

Kotha Gangadhar  <http://orcid.org/0000-0002-0264-2512>

References

- [1] Tan WC, Xu MY. The plane plane suddenly set in motion in a viscoelastic fluid with the Maxwell model. *Acta Mech Sin.* 2002;18:342–349.
- [2] Jamil M, Fetecau C. Helical flows of Maxwell fluid between coaxial cylinders with given shear stresses on the boundary. *Nonlinear Anal Real World Appl.* 2010;5:4302–4311.
- [3] Kumar R, Bhattacharyya A, Seth GS, et al. Transportation of magnetite nanofluid flow and heat transfer over a rotating porous disk with Arrhenius activation energy: fourth order Noumerov's method. *Chin J Phys.* 2021;69:172–185.
- [4] Khan M, Ahmed A, Ahmed J. Boundary layer flow of Maxwell fluid due to torsional motion of cylinder: modelling and simulation. *Appl Math Mech.- Engl Ed.* 2020;41:667–680.
- [5] Kumar RN, Jyothi AM, Alhumade H, et al. Impact of the magnetic dipole on thermophoretic particle deposition in the flow of Maxwell fluid over a stretching sheet. *J Mol Liq.* 2021;334:116494.
- [6] Loenko DS, Shenoy A, Sheremet MA. Effect of time-dependent wall temperature on natural convection of a non-Newtonian fluid in an enclosure. *Int J Therm Sci.* 2021;166:106973.
- [7] Saif RS, Mustafa M, Afzaal MF, et al. Analytical solutions for fluid flow triggered by a melting cylindrical plane in upper-convected Maxwell (UCM) fluid. *Int Commun Heat Mass Transf.* 2021;121:105059.
- [8] Zhang Y, Zhang Y, Bai Y, et al. Flow and heat transfer analysis of a Maxwell-power-law fluid film with forced thermal Marangoni convective. *Int Commun Heat Mass Transf.* 2021;121:105062.
- [9] Cheng L, Nawaz M, Kaneez H, et al. Flow and heat transfer analysis of elastoviscoplastic generalized non-Newtonian fluid with hybrid nanostructures and dust particles. *Int Commun Heat Mass Transf.* 2021;126:105275.
- [10] Pimenta F, Alves MA. Conjugate heat transfer in the unbounded flow of a viscoelastic fluid past a sphere. *Int J Heat Fluid Flow.* 2021;89:108784.
- [11] Dong RY, Dong Y, Sellitto A. An analogy analysis between one-dimensional non-Fourier heat conduction and non-newtonian flow in nanosystems. *Int J Heat Mass Transf.* 2021;164:120519.
- [12] Chaudhary MA, Merkin JH. A simple isothermal model for homogeneous, heterogeneous reactions in boundary layer flow: I equal diffusivities. *Fluid Dyn Res.* 1995;16:311–333.
- [13] Merkin JH. A model for isothermal homogeneous-heterogeneous reactions in boundary layer flow. *Math Comput Model.* 1996;24:125–136.
- [14] Venkata Subba Rao M, Gangadhar K, Chamkha AJ, et al. Bioconvection in a convectational nanofluid flow containing gyrotactic microorganisms over an isothermal vertical cone embedded in a porous plane with chemical reactive species. *Arab J Sci Eng.* 2021;46:2493–2503.
- [15] Ayub A, Sabir Z, Le DN, et al. Nanoscale heat and mass transport of magnetized 3-D chemically radiative hybrid nanofluid with orthogonal/inclined magnetic field along with the rotating sheet. *Case Stud Therm Eng.* 2021;26:101193.
- [16] Khan M, Ahmed J, Ali W. An improved heat conduction analysis in swirling viscoelastic fluid with homogeneous-heterogeneous reactions. *J Therm Anal Calorim.* 2021;143:4095–4106.
- [17] Mishra SR, Mathur P, Ali HM. Analysis of homogeneous-heterogeneous reactions in a micropolar nanofluid past a non-linear stretching plane: semi-analytic approach. *J Therm Anal Calorim.* 2021;144:2247–2257.
- [18] Sheikh M, Abbas Z, Hasnain J, et al. Impact of non-linear Rosseland approximation on the flow of Newtonian fluid with unequal diffusivities of chemically reactive species. *Arab J Sci Eng.* 2021;46:2711–2719.
- [19] Ali M, Sultan F, Shahzad M, et al. Influence of homogeneous-heterogeneous reaction model for 3D cross fluid flow: a comparative study. *Indian J Phys.* 2021;95:315–323.
- [20] Von Kármán T. Über laminare und turbulente Reibung. *Zeitschrift für Angew Math Mech ZAMM.* 1921;1:233–252.
- [21] Cochran EG. The flow due to a rotating disk. *Proc Camb Philos Soc.* 1934;30:365–375.

- [22] Stuart JT. On the effects of uniform suction on the steady flow due to a rotating disk. *Q J Mech Appl Mech.* 1954;7:446–457.
- [23] Ackroyd JAD. On the steady flow produced by a rotating disk with either plane suction or injection. *J. Eng. Math.* 1978;12:207–220.
- [24] Bödewadt UT. Die Drehströmungüberfestem Grund. *Z Angew Math Mech.* 1940;20:241–252.
- [25] Owens JM, Rogers RH. Flow and heat transfer in rotating disk systems. Research Stud. Press Ltd, John Wiley and Sons; 1989.
- [26] Turkyilmazoglu M. MHD fluid flow and heat transfer due to a stretching rotating disk. *Int J Therm Sci.* 2012;51:195–201.
- [27] Khan M, Ahmed J, Ahmad L. Chemically reactive and radiative von Kármán swirling flow due to a rotating disk. *Appl Math Mech.- Engl Ed.* 2018;39:1295–1310.
- [28] Yao G, Zhao J, Shen X, et al. Effects of rheological properties on heat transfer enhancements by elastic instability in von-Karman swirling flow. *Int J Heat Mass Transf.* 2020;152:119535.
- [29] Hafeez A, Khan M. Flow of Oldroyd-B fluid caused by a rotating disk featuring the Cattaneo-Christov theory with heat generation/absorption. *Int Commun Heat Mass Transf.* 2021;123:105179.
- [30] Shehzad SA, Abbas Z, Rauf A, et al. Dynamics of fluid flow through Soret-Dufour impacts subject to the upward and downward motion of rotating disk. *Int Commun Heat Mass Transf.* 2021;120:105025.
- [31] Gangadhar K, Naga Bhargavi D, Venkata Subba Rao M, et al. Entropy minimization on magnetized Boussinesq couple stress fluid with non-uniform heat generation. *Phys Scr.* 2021;96:095205.
- [32] Anwar T, Kumam P, Thounthong P, et al. Nanoparticle shape effects on the thermal performance of Brinkman-type ferrofluid under heat injection/consumption and thermal radiation: A frictional model with non-singular kernel and non-uniform temperature and velocity conditions. *J Mol Liq.* 2021;335:116107.
- [33] Thriveni K, Mahanthesh B. Heat transport of hybrid nanomaterial in an annulus with quadratic Boussinesq approximation. *Appl Math Mech.-Engl Ed.* 2021;42:885–900.
- [34] Shafiq A, Mebarek-Oudina F, Sindhu TZ, et al. A study of dual stratification on stagnation point Walters' B nanofluid flow via radiative Riga plate: a statistical approach. *Eur Phys J.* 2021;136:407.
- [35] Mackolil J, Mahanthesh B. Inclined magnetic field and nanoparticle aggregation effects on thermal marangoni convection in nanoliquid: A sensitivity analysis. *Chin J Phys.* 2021;69:24–37.
- [36] Zhang L, Bhatti MM, Shahid A, et al. Non-linear nanofluid fluid flow under the consequences of Lorentz forces and Arrhenius kinetics through a permeable plane: A robust spectral approach. *J Taiwan Inst Chem Eng.* 2021;124:98–105.
- [37] Khan MN, Nadeem S. Consequences of Darcy-Forchheimer and Cattaneo-Christov on a radiative three-dimensional Maxwell fluid flow over a vertical plane. *J Taiwan Inst Chem Eng.* 2021;118:1–11.
- [38] Khan SU, Tlili I, Waqas H, et al. Effects of non-linear thermal radiation and activation energy on modified second-grade nanofluid with Cattaneo-Christov expressions. *J Therm Anal Calorim.* 2021;143:1175–1186.
- [39] Roohi R, Heydari MH, Bavi O, et al. Chebyshev polynomials for generalized Couette flow of fractional jeffrey nanofluid subjected to several thermochemical effects. *Eng Comput.* 2021;37:579–595.
- [40] VSR M, Gireesha BJ, Gangadhar K, et al. Entropy generation analysis of the electrical magneto-hydrodynamic flow of TiO₂-Cu/H₂O hybrid nanofluid with partial slip. *Int J Numer Method H.* 2021;31(6):1905–1929.
- [41] Ahmad L, Ahmed J, Ahmed A. Thermal energy transport thin film flow over a decelerating rotating disk. *Proc Inst Mech Eng E: J Prodess Mech Eng.* 2022;236(2):491–499.
- [42] Ahmad L, Ahmed J, Khan M, et al. Effectiveness of Cattaneo-Christov double diffusion in Sisko fluid flow with variable properties: dual solutions. *J Therm Anal Calorim.* 2021;143(5):3643–3654.
- [43] Ahmad J, Khan M, Ahmad L. Effectiveness of homogeneous-heterogeneous reactions in Maxwell fluid flow between two spiraling disks with improved heat conduction features. *J Therm Anal Calorim.* 2020;139:3185–3195.

- [44] Ahmad L, Munir A, Khan M. Locally non-similar and thermally radiative Sisko fluid flow with magnetic and Joule heating effects. *J. Magn Magn Mater.* **2019**;487:165284.
- [45] Ahmad L, Khan M, Khan WA. Numerical investigation of magneto-nanoparticles for unsteady 3D generalized Newtonian liquid flow. *Eur Phys J Plus.* **2017**;132:373.
- [46] Ahmad L, Khan M. Numerical simulation for MHD flow of Sisko nanofluid over a moving curved surface: A revised model. *Microsyst Technol.* **2019**;25:2411–2428.
- [47] Ahmad L, Khan M. Importance of activation energy in development of chemical covalent bonding in flow of Sisko magnetonanofluids over porous moving curved surface. *Int J Hydrog Energy.* **2019**;44(21):10197–10206.
- [48] Fisher RA. On the “probable error” of a coefficient of correlation deduced from a small sample. *Metron.* **1921**;1:03–32.
- [49] Fang T. Flow over a stretchable disk. *Phys Fluids.* **2007**;19:128105.
- [50] Mahanthesh B, Shehzad SA, Ambreen T, et al. Significance of Joule heating and viscous heating on heat transport of MoS₂-Ag hybrid nanofluid past an isothermal wedge. *J Therm Anal Calorim.* **2021**;143:1221–1229.